Journal of the European Ceramic Society 22 (2002) 933–945

www.elsevier.com/locate/jeurceramsoc

Dissolution of Eu^{3+} cations in mesopores in amorphous Al_2O_3 and controlled reconstructive nucleation and growth of γ-Al_2O_3 nanoparticles

P. Mohanty, S. Ram*

Materials Science Centre, Indian Institute of Technology, Kharagpur-721302, India

Received 2 November 2000; received in revised form 22 June 2001; accepted 9 July 2001

Abstract

Dispersed Eu^{3+} cations in an aqueous $EuCl_3$ solution easily incorporate in pores in a hydrogenated porous $AlO(OH)\cdot\alpha H_2O$ boehmite powder. H_2 gas in pores and OH^- anions from energized boehmite with pores covert $EuCl_3$ into Eu_2O_3 in pores as per the reaction, $2\ EuCl_3 + \frac{3}{2}H_2 + 3\ OH^- \rightarrow Eu_2O_3 + 6\ HCl$, in a closed reactor at room temperature. This is a very efficient spontaneous exothermic reaction which occurs with evolution of H_2 gas and HCl vapour as per experimental conditions. The obtained Eu^{3+}:Al_2O_3 product consists of dispersed Eu_2O_3 nanoparticles (D$\sim$30 nm crystallite size) in an amorphous Al_2O_3 in a mesoporous structure. On heating, Eu_2O_3 nanoparticles dissolve in high surface energy pores and result in a complete amorphous structure of Eu^{3+}: Al_2O_3 at $\sim$700 K. A controlled reconstructive nucleation and growth into γ-Al_2O_3 nanoparticles in D$\sim$6.5 nm occurs from the amorphous state at $\sim$1000 K. Several batches of the reaction, with Eu^{3+} contents up to 1.5 wt.%, have been carried out and all of them have a complete dissolution of Eu^{3+} cations in Al_2O_3 at these temperatures. The results are analyzed in terms of X-ray diffraction, microstructures, and IR spectra of samples prepared under different conditions.

Keywords: Eu_2O_3; γ-Al_2O_3; Porosity; Nanocomposites; Optical devices; Powders-solid state reaction

1. Introduction

Doped Al_2O_3 with a small amount of Eu^{3+} cations, of the order of 1 wt.% or so, forms an important material for lasers, phosphors, optical sensors, and other devices.[1,2] Its optical characteristics depend on its microstructure. An amorphous structure of dispersed Eu^{3+} in an Al_2O_3 host promises activated optical properties with an improved quantum efficiency. Several reports are available on doped Eu^{3+} in borate and other oxide glasses.[2–6] However, fabrication of Eu^{3+}:Al_2O_3 in an amorphous Eu^{3+} structure is not common. Conventional methods of solid state reaction, glass melting, or sol gel chemistry, often used to obtain an amorphous ceramic structure,[2–6] are not suitable to obtain it without inducing a significant devitrification. The precursor in these methods often involve a high processing temperature at which its components either appear in two independent crystalline phases or react together and result in a compound in a complex structure of aluminate, garnet, or others.[1,7] Formation of an Eu^{3+}:Al_2O_3 glass by melting and casting needs as high temperature as $\sim$2300 K.[8] It fails to retain its vitreous structure on cooling through such a large temperature range to room temperature or its glass transition temperature.

A solid state dissolution of Eu^{3+} cations in a porous Al_2O_3 is explored as an alternative way of preparing a doped Eu^{3+}:Al_2O_3 sample at moderate temperature in this article. This is a new method of its type. It permits dissolution of otherwise even immiscible cations in the high energy pores.[9,10] There has been interest in studying solid state amorphization SSA reactions.[11] An amorphous phase can be formed when a crystalline solid is subjected to various types of disordering processes. The reactions are governed by their thermodynamics as well as kinetic factors.[12] The excess Gibbs free energy ΔG caused by reactions of crystallites at a high energy surface acts as the driving force for the

* Corresponding author. Tel.: +91-3222-83980; fax: +91-3222-55303.

E-mail address: sram@matsc.iitkgp.ernet.in (S. Ram).

0955-2219/02/$ - see front matter
PII: S0955-2219(01)00390-9

crystalline to amorphous state transformation. A nucleation and growth from the amorphous state may occur during the reaction. It results from the interplay between the thermodynamic driving forces, reaction kinetics, and the ease of nucleation of the competing phase(s).

The nucleation of an amorphous phase often takes place at defect sites in the lattice of the slow moving species, and its growth is determined by diffusivity of the fast moving species through the already-grown interfaces. It involves an interesting phenomenon of its asymmetric growth.[13–15] The defects sites for the asymmetric growth of the amorphous phase must have a certain level of excess ΔG, for that SSA reaction could not be observed either at single crystals or at low-angle grain boundaries.[11] The heat of formation and atomic size mismatch are two important factors to determine amorphous phase formation in a system.[16]

In this article, we report the results of incorporation of Eu^{3+} cations in a mesoporous Al_2O_3 host and their SSA reaction with the pores. The SSA reaction occurs on annealing the specimen at moderate temperature as 650 K. The results are analyzed in terms of X-ray diffraction, microstructures, and infrared spectra of representative samples before and after annealing at elevated temperatures. Excess ΔG in interface between pore wall and particles, S_1, and free surface of particles in pores, S_2, is used to model the SSA reaction.

2. Experimental details

2.1. Synthesis

The sample of dispersed Eu^{3+} cations (oxide) in Al_2O_3 matrix is prepared by reaction of an aqueous $EuCl_3.6H_2O$ solution with a hydrogenated porous AlO(OH).αH_2O powder in a closed reactor at room temperature. A freshly prepared $AlO(OH)\cdot\alpha H_2O$ powder, with an initial porosity $\Phi = 90\%$ and 10–50 nm average pore diameter d, was used. It was obtained by an electrochemical surface hydrolysis of Al-metal in a humid air.[17]

On adding a solution of $EuCl_3\cdot 6H_2O$, in 0.1–0.01 M concentration, to the porous $AlO(OH)\cdot\alpha H_2O$ powder dropwise while stirring the mixture, Eu^{3+} cations travel to and occupy the pores. A reaction occurs with pores and converts $EuCl_3$ into Eu_2O_3. Hydrogenated pores promote the reaction at room temperature. It is an exothermic reaction which occurs with evolution of H_2 gas and water/HCl vapour. Ultimately, a paste of dispersed Eu_2O_3 in the matrix of Al_2O_3, obtained by decomposition of $AlO(OH)\cdot\alpha H_2O$ on the reaction, is formed. The obtained sample is washed with water and then dried in air at ~450 K. The dried powder has a characteristic grayish white colour.

On heating, Eu_2O_3 particles dissolve in pores in Al_2O_3 and a completely amorphous structure of Eu^{3+}: Al_2O_3 results at ~700 K. A reconstructive nucleation and growth of γ-Al_2O_3 nanoparticles occurs from the amorphous state at temperature as small as 850 K. Several batches of the reaction, with Eu^{3+} contents up to 1.5 wt.%, have been carried out in this way and all of them have a complete Eu_2O_3 dissolution in the matrix at these temperatures. Colour of the sample has changed from grayish to whitish.

2.2. Measurements and analysis

The microstructure is studied with a scanning electron microscope (SEM) of JEOL model-840 and a transmission electron microscope (TEM) of Hitachi H-600. Phase analysis of the samples before and after the reaction at selected temperatures is carried out with X-ray powder diffraction. The diffraction has been recorded with P. W. 1710 diffractometer using filtered CoK radiation of wavelength $\lambda = 0.17905$ nm. The Φ has been estimated by N_2 gas isothermal sorption at liquid N_2 temperature using Quantachrome Autosorb-1[18] and by difference in specific density of the sample from the theoretical value. Thermal decomposition of Eu^{3+}:AlO(OH)$\cdot\alpha H_2O$ and the chemisorption of adsorbed gases in the porous Eu^{3+}:Al_2O_3 powder were analyzed with thermogravimetric analysis TG. A Perkin-Elmer thermal analyzer was used to recorded the TG thermogram by heating 10–20 mg sample (in argon atmosphere) over 300–1000 K at 20 K/min heating rate.

IR spectrum (400–4000 cm^{-1}) is recorded of powder compacted in form of a pellet in KBr matrix. The data is collected with a Shimazuir 470 infrared spectrophotometer. The reported frequencies are accurate to ± 2 cm^{-1} in the case of sharp bands and ± 5 cm^{-1} or even larger in the case of broad bands. Other details are the same as reported earlier.[19]

3. Results and discussion

3.1. Reaction process

The hydrogenated porous $AlO(OH)\cdot\alpha H_2O$ powder behaves as a reducing agent. It coverts $EuCl_3$ to Eu_2O_3 as soon as it is added and dispersed in the pores. The reaction is exothermic as can be seen by 5–10 K increase in average temperature of the mixture as per the experimental conditions. The local temperature in the reaction centres may be higher, i.e. as much as the B.P. of water or even more, i.e. sufficient enough to cause in situ decomposition of AlO(OH) into Al_2O_3. It occurs with evolution of H_2 gas and some water/HCl vapour. The evolution of H_2 gas can be observed by bubbling it through water in a beaker. It burns with a flame if

putting a burning stick and turns up colour of a blue litmus paper to red.

The reaction with energized AlO(OH) in the pores, which involve a high surface energy, can be expressed as follows,

$$2\ EuCl_3 + 6\ AlO(OH) \rightarrow Eu_2O_3 + 3\ Al_2O_3 + 6\ HCl \quad (1)$$

The H_2 gas, which occupies the pores in the hydrogenated powder, possibly exists in an ionized form at pore surface. This promotes the reaction by raising the total Gibb's free energy G of the powder. A porous powder has a lot of vacancy defects and those could be occupied by H^+ cations. These high energy H^+ cations form hydronium ions $[H_3O]^+$ by reacting with internal H_2O molecules in the powder. The $[H_3O]^+$ ions have an activated reaction (1),

$$H_2O + H^+ \rightarrow [H_3O]^+$$

$$2\ EuCl_3 + 3\ [H_3O]^+ \rightarrow Eu_2O_3 + 6HCl + \frac{3}{2}H_2 \uparrow \quad (2)$$

It is this hydrogen which releases along with HCl and H_2O vapour during the reaction. This is useful in conducting an internal co-reduction or an ion exchange reaction in a mesoporous composite with desirably doped metal or metal cations in pores.

The product in reactions (1) and (2) results in a paste of dispersed Eu_2O_3 in Al_2O_3 with residual HCl and H_2O byproducts. Part of the HCl dissolves part of the precursor by forming $AlO(OH).\alpha H_2O + 3\ HCl \rightarrow AlCl_3 + (\alpha + 2)\ H_2O$, which goes to the solution as it is soluble in water. In a controlled reaction with a limited $EuCl_3$, as in this example, the total amount of the HCl produced is also small. Most of it is consumed in the above reaction and hardly succeeds to dissolve a significant part of the final product of Eu_2O_3 back to $EuCl_3$, i.e.

$$Eu_2O_3 + 6\ HCl \rightarrow 2\ EuCl_3 + 3\ H_2O \quad (3)$$

In case any $EuCl_3$ forms in reaction (3) goes back to the solution as the reactant. The byproduct Cl^- ions impurities are easily removed by washing in distilled water. No impurities of them have been found by a chemical test with $AgNO_3$ in the sample recovered in this way. On heating at ~450 K, the H_2O with traces of HCl, if any, evaporates out leaving behind a dried Eu^{3+}:Al_2O_3 powder. The dried sample appears in a grayish white characteristic colour.

3.2. X-ray diffraction analysis

3.2.1. Incorporation of Eu^{3+} cations in pores

Incorporation of Eu^{3+} cations in pores in the porous $AlO(OH)\cdot\alpha H_2O$ powder can be analyzed from X-ray diffraction of the specimen before and after charging by the Eu^{3+} cations. For example, Fig. 1 compares x-ray diffractograms of the samples obtained with different amounts of (a) 0.5, (b) 1.0 and (c) 1.5 wt.% Eu^{3+}. All the three diffractograms have sharp peaks superposed over a weak scattering background between 20 and 100° at 2θ scale. Integrated intensity in these peaks is increasing in proportination to the Eu^{3+} contents. The most intense peak (peak intensity $I_p = 100$ units) of the diffractogram appears at 0.3146 nm with the second intense peak at 0.4111 nm, $I_p = 60$ units, in Fig. 1a. The I_p regularly increases in the second peak with an increase in Eu^{3+} content so that it becomes a more or less the same as in the most intense peak in Fig. 1c. Another peak at 0.2711 nm has a similar result of its increasing I_p as a function of Eu^{3+}content. This indicates a functional orientational ordering of Eu^{3+} cations in a crystal lattice in pores. No such peaks appear from the Al_2O_3 matrix confirming its amorphous structure. Amorphous Al_2O_3 permits Eu^{3+} ordering in pores by decreasing the total G value.

The above X-ray diffractogram differs the diffraction in $EuCl_3\cdot 6H_2O$ in the $P6_3/m$ hexagonal crystal structure.[20] In that case, the most intense peak occurs in (201) reflection at 0.2526 nm with the second and third intense peaks in (211) and (101) reflections at 0.2084 and 0.3469 nm, respectively. The most intense peak in the present case, e.g. in 0.5 wt.% Eu^{3+} sample, is at an enhanced value of (201) peak by 1.25% at 0.3146 nm while the second and third intense peaks appear at 0.4111 and 0.2060 nm, respectively. $EuCl_3\cdot 6H_2O$ has no peak around 0.3146 nm and only a weak peak at 0.2066 nm.[20]

The X-ray diffractogram in Fig. 1 is fairly matching with the standard diffractogram of the C_2/m monoclinic Eu_2O_3 with lattice parameters $a = 1.4042$ nm, $b = 0.3638$ nm, $c = 0.8746$ nm and $\beta = 100°7'$.[21] On increasing the Eu^{3+} content from 0.5 to 1.5 wt.%, the values of a, b and c are regularly increased according to an enhanced lattice volume V_0 as much as 0.4%. The increase in V_0 is indicative of generation of a high energy interface of Eu^{3+} with Al_2O_3 on increasing its volume in pores. The high energy interface causes a lattice strain which results in the manifested V_0 value. It supports a high energy amorphous structure of the Al_2O_3 matrix characterized by a broad and weak diffraction halo at wavevector $q = 45$ nm^{-1} in Fig. 2a. This diffraction halo is masked in strong diffraction of crystalline Eu_2O_3 phase in Fig. 1.

3.2.2. Dissolution of Eu_2O_3 in pores on thermal annealing

On heating, the high energy interface of Eu^{3+} with Al_2O_3 in divided pores destabilizes crystalline structure of Eu^{3+} by propagation of the high energy lattice strain. As a result, Eu^{3+} crystallites dissolve in pores through Al_2O_3 in intimate contact, forming a solid Eu^{3+}:Al_2O_3

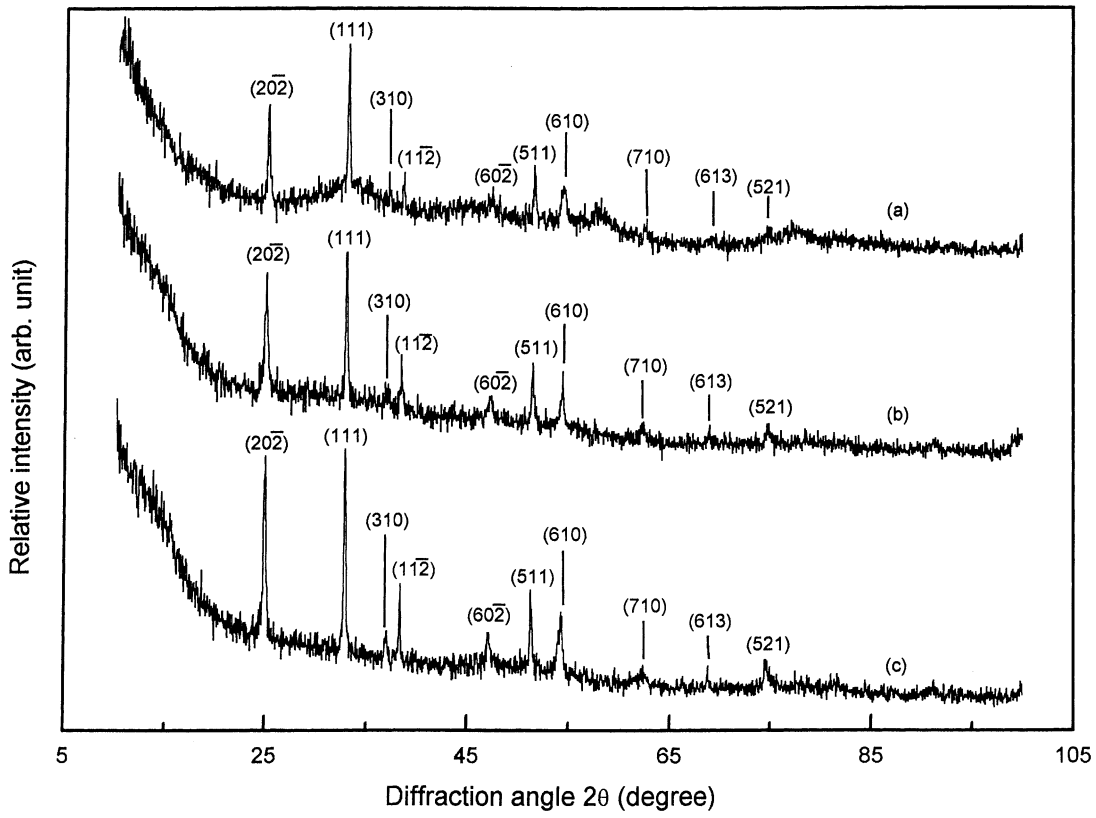

Fig. 1. X-ray diffraction of Eu^{3+} doped mesoporous Al_2O_3 powders: (a) 0.5, (b) 1.0 and (c) 1.5 wt.% Eu^{3+}. The Al_2O_3 matrix has an amorphous structure. The samples have been dried at 450 K after washing the reacted powder in water.

solution. It occurs at expense of the excess ΔG or volume ΔV by annihilation of pores. It passes through a series of nonequilibrium high energy metastable states of internal energy ε far larger than in an ordered thermodynamic equilibrium state in a crystalline solid in this series. As a result, the resulting solid solution passes through an intermediate amorphous structure. A complete amorphous structure, characterized by a broad halo at $q = 45\ nm^{-1}$, appears in the sample with 1.5 wt.% Eu^{3+} on annealing at $\sim$700 K (Fig. 2a). A recrystallization from the amorphous state starts at as early temperature as 850 K. Annealing at 1000 or 1100 K (Fig. 2b or c) results in a crystalline phase of γ-Al_2O_3 with lattice parameter $a = 0.7890$ nm, which is smaller in comparison to the $a = 0.7924$ bulk value,[22] in O_H^7–F_{D3M} cubic crystal structure. An average crystallite size $D = 6.5$ nm is calculated using bandwidths, $\Delta 2\theta_{1/2}$, in the characteristic peaks in the Debye–Scherrer relation[23] in the two samples. The Eu^{3+} dissolved in the amorphous Al_2O_3 does not recrystallize at these temperatures.

A comparison of X-ray diffractograms of (a) the pure and doped samples with (b) 0.5, (c) 1.0, and (d) 1.5 wt.% Eu^{3+} in Fig. 3 envisages that the Eu^{3+} promotes γ-Al_2O_3 grain growth at 1100 K. The average values for D and a obtained from $\Delta 2\theta_{1/2}$ and d_{hkl} (interplanar spacing) in the characteristic diffraction peaks are given in Table 1. As per the Eu^{3+} content, the D value varies between 4.0 and 6.5 nm while the a value varies between 0.7915 and 0.7882 nm, with a maximal 0.7915 nm value at $D = 4.0$ nm in sample (b). A minimal $a = 0.7882$ nm value has been found at $D = 4.5$ nm in sample (a), which has no Eu^{3+} content. The a value varies in this series governed by a combined effect of (i) quantum confined size effect in small crystallites[24–26] and (ii) the lattice strain (leads to enhance the a value) induced by formation of the Al_2O_3 solid solution with Eu^{3+} additives.

Owing to large size (radius $r = 0.1087$ nm) as almost twice the Al^{3+} ($r = 0.0530$ nm) size,[27] Eu^{3+} hardly prefers partial substitution of Al^{3+} in Al_2O_3 crystal lattice. In order to analyze it, we explored high resolution X-ray diffractograms in γ-Al_2O_3 lattice reflections. The diffractograms obtained in (400) and (440) reflections from annealed samples at 1100 K for 2 h are portrayed in Figs. 4 and 5. (400) reflection, which appears at 0.1972 nm in virgin γ-Al_2O_3 in Fig. 4a, is shifted a very little at larger 0.1979 nm value on incorporating 0.5 wt.% Eu^{3+}. A more pronounced shift in the peak position occurs in (440) reflection. It occurs at 0.1392 nm in virgin sample in Fig. 5a and shifts at 0.1400 nm along with 20% decrease in the $\Delta 2\theta_{1/2}$ value on the 0.5 wt.% Eu^{3+} addition in Fig. 5b. An adverse effect on shift in the diffractogram at lower d_{hkl} value at 0.1394 or 0.1391 nm occurs at a larger 1.0 or 1.5 wt.% Eu^{3+} content in

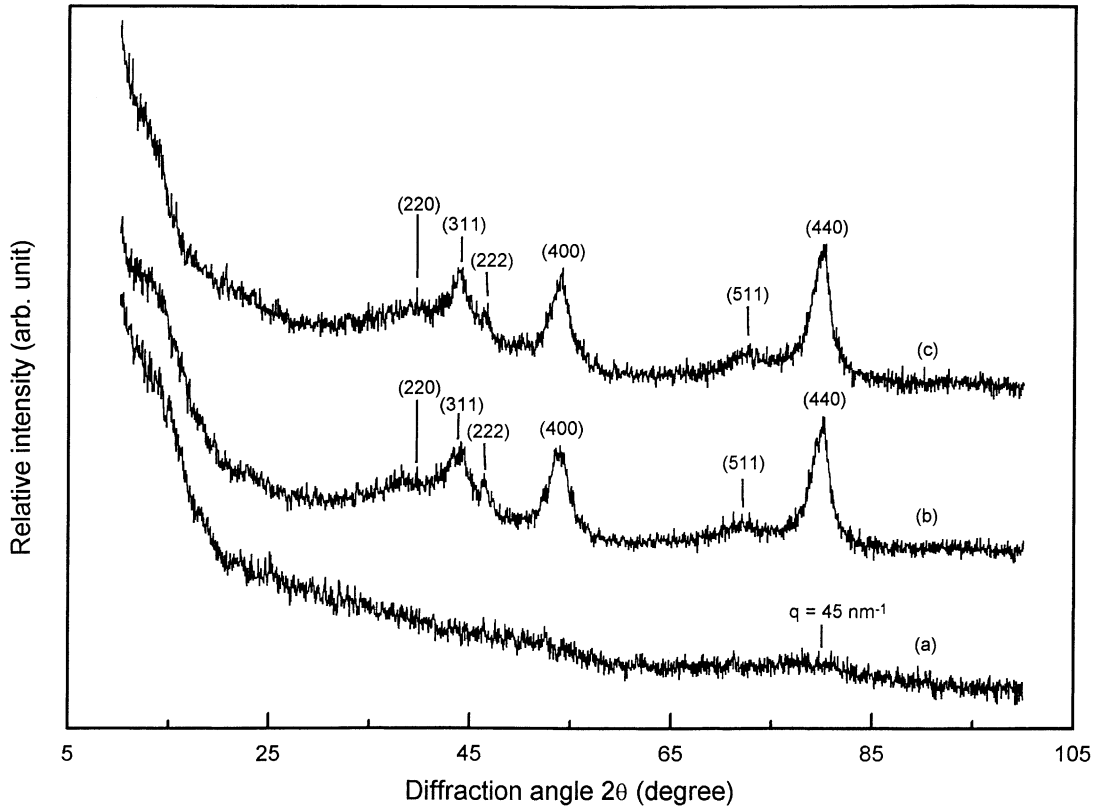

Fig. 2. X-ray diffraction showing the effects of thermal annealing of 1.5 wt.% Eu^{3+}:Al_2O_3 powder in air at (a) 700 K, (b) 1000 K, and (c) 1100 K for 2 h.

other samples in Fig. 5c or d. It reflects in a significant decrease in the $\Delta 2\theta_{1/2}$ value by 40 and 50%, respectively, relative to the virgin sample value. The results indicate a significant Eu^{3+} substitution on Al^{3+} sites in (440) plane in γ-Al_2O_3. As expected, the substitution seems to saturate as early as at 0.5 wt.% Eu^{3+} addition through this process.

3.3. Thermogravimetric analysis

Fig. 6 shows part of (a) TG thermogram and (b) its derivative DTG obtained during heating the 1.5 wt.% Eu^{3+}:Al_2O_3 powder at 20 K/min heating rate. The sample has been dried in air at ~450 K after the processing. According to these curves, the sample has a huge mass loss of a total of 41% over 300–700 K. It occurs in two distinct steps in the regions of AB and BC as marked over the TG curve. This confirms indirectly a huge Φ present in the sample in a mesoporous structure. A similar TG desorption curve, with 21% mass loss,[17,18] appears in Al_2O_3 powder without the doping.

A value of $\Phi \sim 40\%$ is determined by difference in the experimental $\rho = 1.5$ g/cm^3 and theoretical $\rho = 2.5$ g/cm^3 values of density of the sample. It is confirmed further by measuring its capacity of N_2 gas sorption by the standard method. In this experiment, the sample was first degassed at a reduced pressure $\sim 10^{-5}$ bar and then N_2 gas has been loaded to ambient pressure. Volume of the adsorbed N_2 gas is measured by isothermal desorption at liquid N_2 temperature. A cylindrical pore shape has been assumed for the pore size distribution, $d = 3-10$ nm, as per the TEM microstructure discussed below.

Table 1
The average crystallite size and lattice parameter for γ-Al_2O_3 recrystallized from the mesoporous Eu^{3+}:Al_2O_3 powders[a]

Eu^{3+} content (wt.%)	Crystallite size (mm)	Lattice parameter (nm)
0.0	4.5	0.7882
0.5	4.0	0.7915
1.0	5.5	0.7896
1.5	6.5	0.7890

[a] Samples have been annealed at 1100 K for 2 h. A significantly larger value of lattice parameter $a = 0.7924$ appears in bulk γ-Al_2O_3.[22]

The two distinct TG desorption signals are more clearly visualized with two distinct peaks at 390 and 515 K in the DTG curve (Fig. 6b). Both of them ascribe the desorption of chemisorbed species in the sample. Those are definitely due to the chemisorbed N_2 and O_2 (or CO_2) gases and moisture from the air. The open pores as well as the large surfaces in the high energy nano-

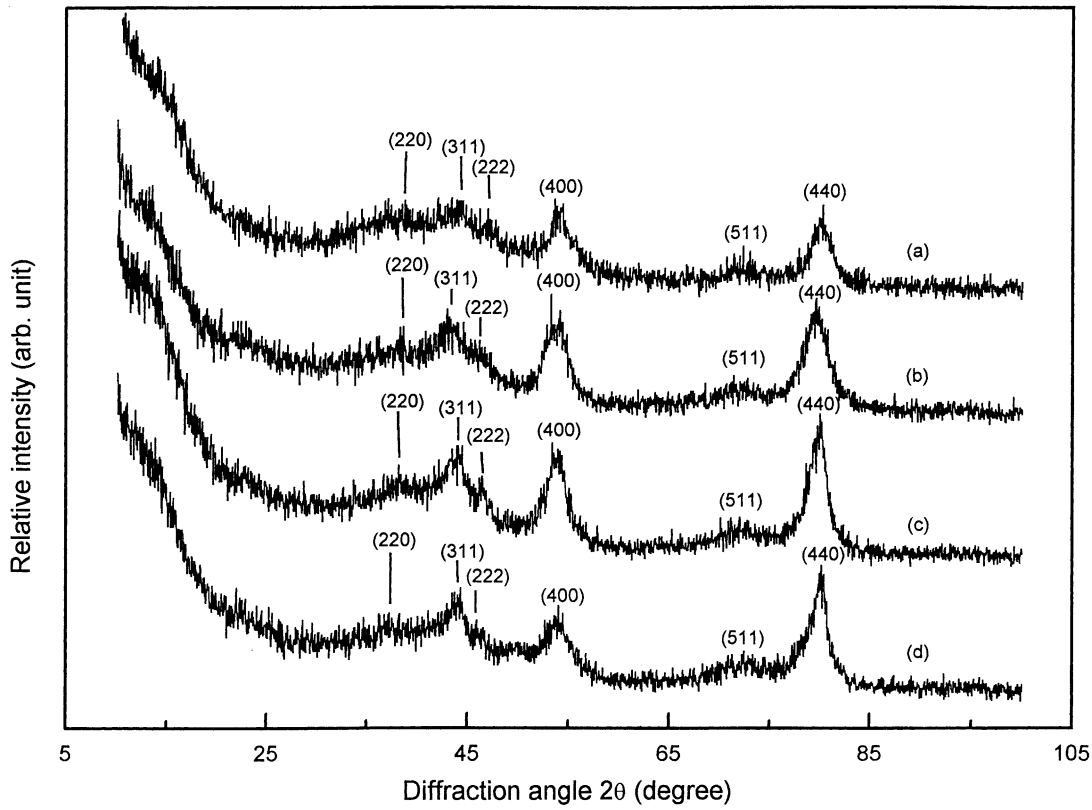

Fig. 3. X-ray diffraction showing the effects of (a) 0.0, (b) 0.5, (c) 1.0, and (d) 1.5 wt.% Eu^{3+} addition in Eu^{3+}:Al_2O_3 powders by annealing in air at 1100 K for 2 h.

particles arranged through the high energy pores act as active centres to adsorb a plenty of such molecular species in this example. The N_2 and O_2 (or CO_2) molecules occupying the pores release rather easily, primarily in the first signal at 390 K, on heating over the early temperatures. The other signal thus arises primarily in the desorption of the residual gas molecules with H_2O molecules from the particle surfaces. These gases easily adsorb in association with H_2O molecules and exist at high energy surfaces to a rather high temperature.

3.4. Microstructure

SEM micrographs for the 1.5 wt.% Eu^{3+}:Al_2O_3 sample are compared in Fig. 7. The micrograph (a), obtained from as dried powder at 450 K, indicates shining particles of Eu_2O_3 (confirmed by in situ electron microprobe analysis) dispersed in thin layers of amorphous Al_2O_3 in 50 nm or still smaller thickness. Average size in small particles is of the order of 100 nm and most of them are in a near spherical shape. This is in an order of larger D value as per $\Delta 2\theta_{1/2}$ in the X-ray diffraction peaks (Fig. 1). This means that most of the Eu_2O_3 particles visible at this scale are clusters of smaller crystallites. The clusters are as big as a few micrometers and appear in bright intense irregular shapes embedded in Al_2O_3 layers.

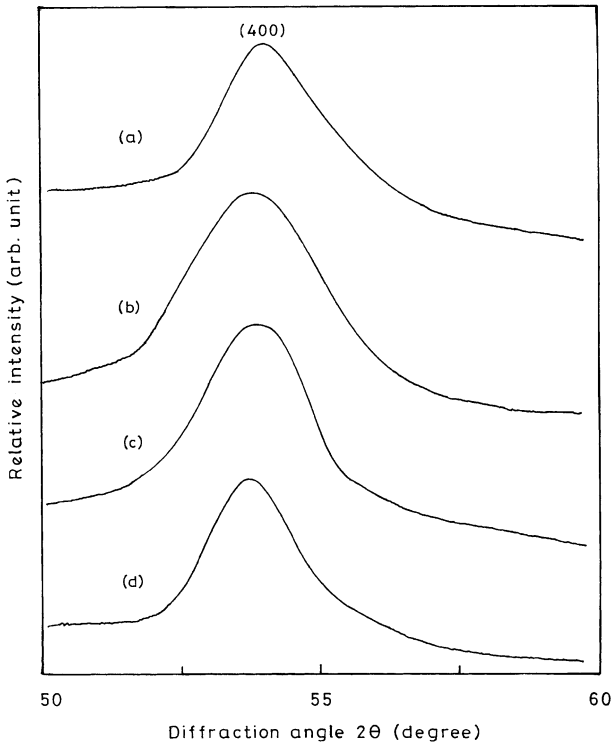

Fig. 4. High resolution X-ray diffractograms in (400) reflection of γ-Al_2O_3 after dissolving (a) 0.0, (b) 0.5, (c) 1.0, and (d) 1.5 wt.% Eu^{3+} in Eu^{3+}:Al_2O_3 at 1100 K. The Eu^{3+} cations are adding a significant peak broadening at 0.5 wt.% Eu^{3+} in (b).

As mentioned above, the Eu_2O_3 particles locally dissolve in the high energy amorphous Al_2O_3 layers subject to heating at 650 K or larger. It results in a peculiar honeycomb type interconnected structure in micrograph (Fig. 7b) for the sample annealed at 1100 K for 2 h. The interconnected structure easily extends over a dimension as large as 250 μm. We tried to have a resolved structure at a higher magnification, but the sample, unfortunately, gets deformed by charging and moves under the electron beam. The charged sample, so called "moving alumina", has a modified microstructure as reproduced

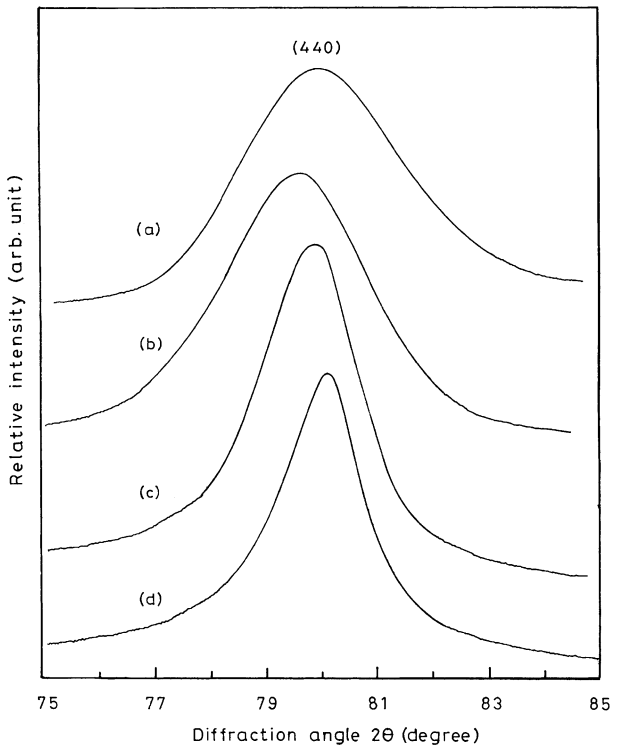

Fig. 5. High resolution X-ray diffractograms in (440) reflection of γ-Al_2O_3 after dissolving (a) 0.0, (b) 0.5, (c) 1.0, and (d) 1.5 wt.% Eu^{3+} in Eu^{3+}:Al_2O_3 at 1100 K. A significant band narrowing and peak shift at lower 2θ-values reappears above 0.5 wt.% Eu^{3+} addition.

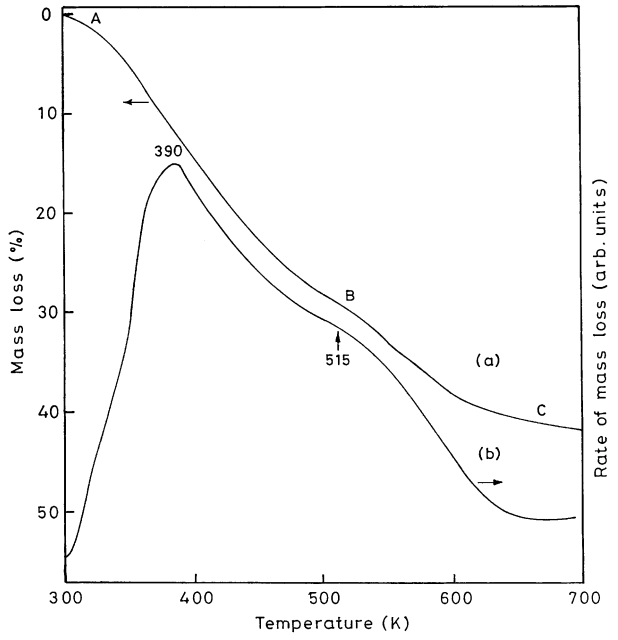

Fig. 6. (a) TG and (b) DTG thermograms for 1.5 wt.% Eu^{3+}:Al_2O_3 mesoporous powder (dried at 450 K after the reaction) at a heating rate of 20 K/min.

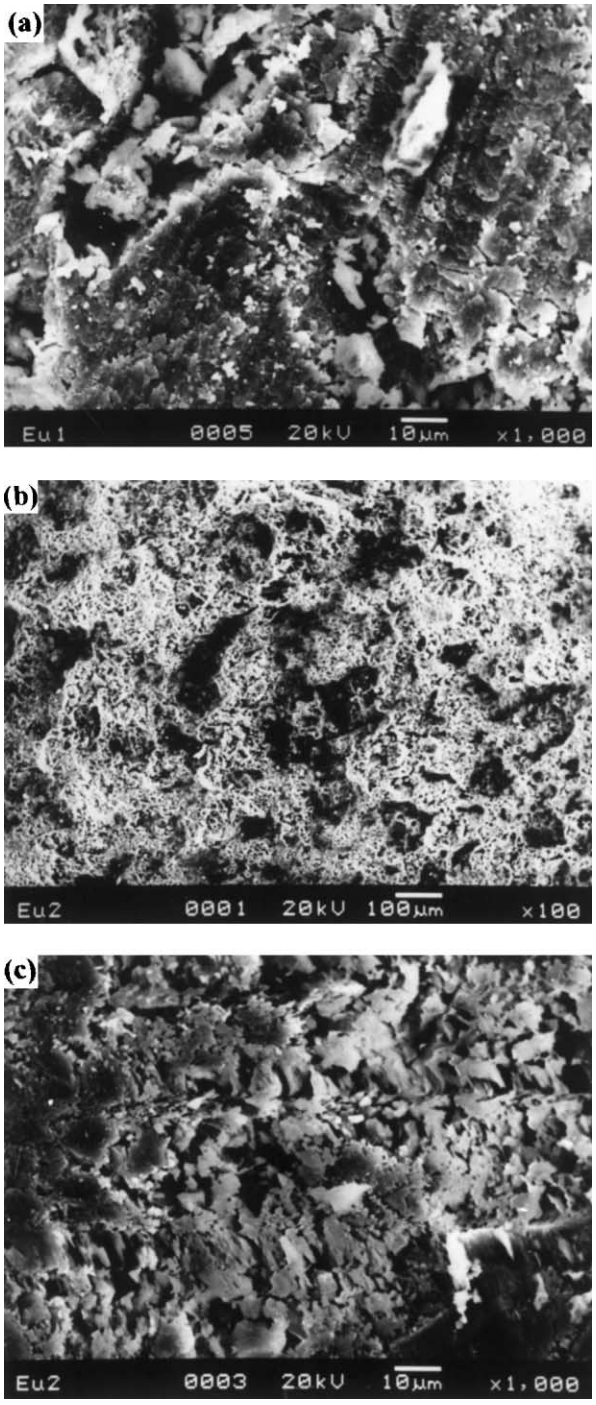

Fig. 7. Scanning electron micrographs of 1.5 wt.% Eu^{3+}: Al_2O_3 powder; (a) dried at 450 K and (b) or (c) annealed at 1100 K for 2 h. Micrographs (b) and (c) are taken at two different magnifications.

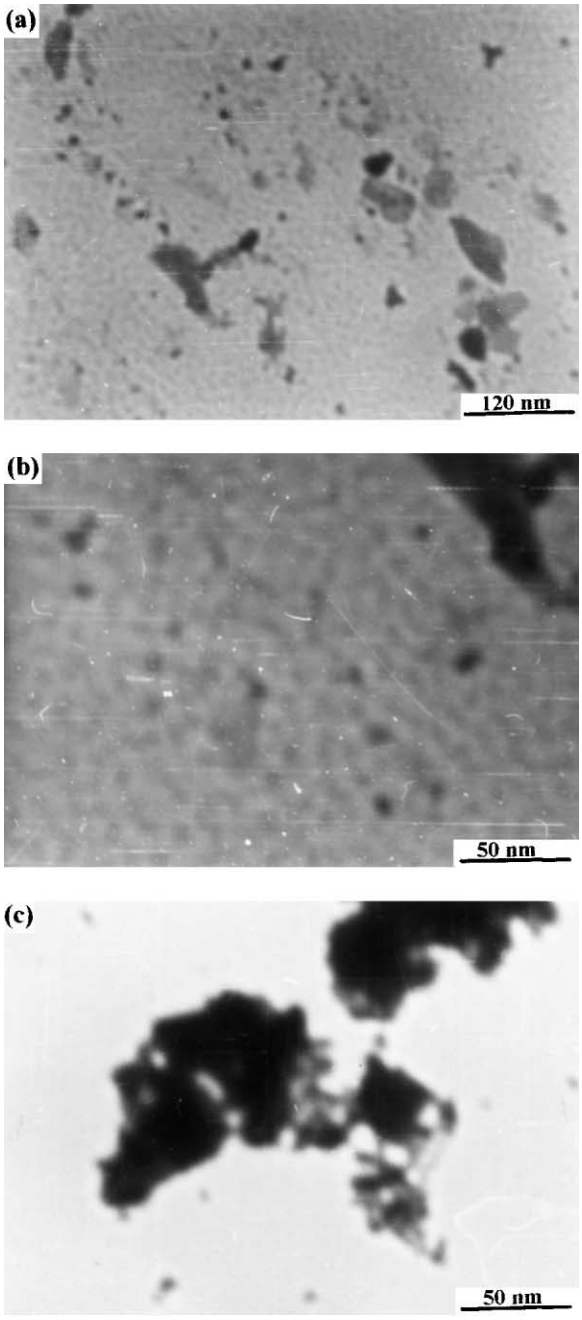

Fig. 8. TEM micrographs for the mesoporous 1.5 wt.% Eu^{3+}:Al_2O_3 powder; (a) or (b) dried at 450 K and (c) annealed at 700 K for 2 h. Micrographs (a) and (b) are taken at two different magnifications.

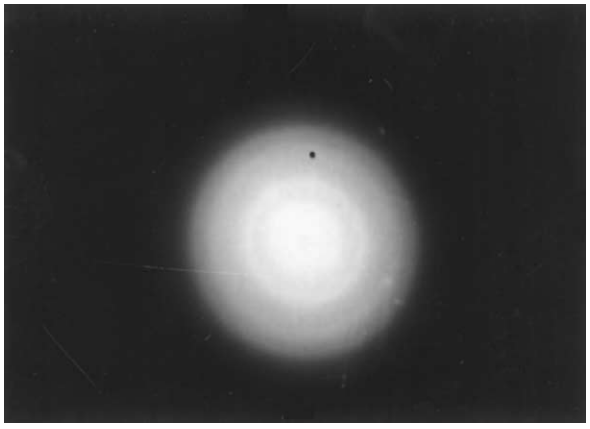

Fig. 9. The electron diffraction corresponding to TEM in Fig. 8(b) for the mesoporous 1.5 wt.% Eu^{3+}:Al_2O_3 powder dried at 450 K.

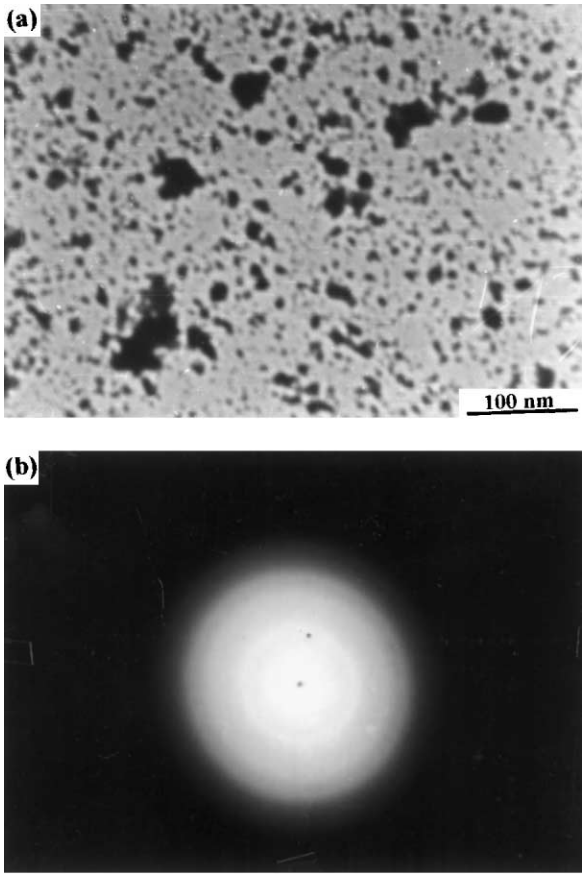

Fig. 10. (a) TEM micrograph and (b) the corresponding electron diffraction for the mesoporous 1.5 wt.% Eu^{3+}:Al_2O_3 powder after annealing at 1100 K for 2 h.

in Fig. 7c. The heating with electron beam causes a disordered Al_2O_3 structure. As a result, it is thinned itself in further thin layers as in the virgin sample in Fig. 7a. The thin layers extend over a refined and reorganized 2–10 μm dimension in a thickness of the order of 50 nm or smaller.

The distribution of Eu_2O_3 crystallites and mesopores that lie at a smaller scale can be studied with their TEM. For example, Fig. 8 compares TEM micrographs for the 1.5 wt.% Eu^{3+}:Al_2O_3 powder before (a) or (b) and after annealing (c) at 700 K for 2 h. Micrographs (a) and (b) are portrayed at two different magnifications to compare the resolved features. Small particles (dark contrast), $D = 2-5$ nm, which are distributed through pores (white contrast), $d = 2-5$ nm, in a specific manner are due to the self-arranged parent Al_2O_3 in a mesoporous structure. Larger pores are derived by combination of

the small ones. The deep dark contrasts represent Eu_2O_3 crystallites in relatively bigger sizes. In micrograph (a), their size varies from 10 to 40 nm. This is consistent with the average $D = 30$ nm value determined from $\Delta 2\theta_{1/2}$ values. Possibly, extremely small crystallites, $D \leqslant 20$ nm, are not in a significant number to impart an effective D or $\Delta 2\theta_{1/2}$ value. The electron diffraction (Fig. 9) has three rings at 0.317, 0.195 and 0.159 nm interatomic distances in (111), (610) and (613) reflections in agreement with the values at 0.317, 0.196 and 0.158 nm in the X-ray diffraction in Fig. 1c.

A fairly sharp reorganized $d \sim 10$ nm size distribution (Fig. 8c) appears in unoccupied pores on dissolving the Eu_2O_3 crystallites in an amorphous 1.5 wt.% Eu^{3+}:Al_2O_3 structure at 700 K. Recrystallization from the latter at 1100 K results in refined γ-Al_2O_3 crystallites in Fig. 10a with the same $D \sim 6.5$ nm value as determined from $\Delta 2\theta_{1/2}$ values (Fig. 3d). The electron diffraction (Fig. 10b) has three rings at 0.239, 0.140 and 0.115 nm interatomic distances in (311), (440) and (444) γ-Al_2O_3 reflections, respectively. They compare well the values at 0.238, 0.139 and 0.114 nm in the X-ray diffraction within the experimental errors.

3.5. IR spectrum

Fig. 11 compares IR spectra of (a) the porous AlO(OH)·αH_2O and (b) 0.5, (c) 0.5, and (d) 1.5 wt.% Eu^{3+} doped Al_2O_3. Spectrum (b) is from the as dried sample at 450 K while that of (c) or (d) is measured after the annealing at 1100 K. The bands appear in three distinct (i) 400–1250 cm^{-1}, (ii) 1300–1800 cm^{-1}, and (iii) 2500–4000 cm^{-1} groups. As expected, their positions as well relative intensities vary with Eu^{3+} additions in spectra (b)–(d) if compared to those in spectrum (a). Some of the characteristic bands of (a) have disappeared and several new bands have developed in these spectra as follows.

Two strong bands, which appear at 976 and 1022 cm^{-1} in AlO(OH).αH_2O, no longer appear in other samples. Both of them are assigned to Al=O stretching vibration in AlO(OH) as it exists in two conformers in amorphous state.[28] Three conformers exist in nanocrystals with three Al=O stretching bands in a more or less the same intensity at 980, 1025 and 1075 cm^{-1}.[28] Only one Al=O stretching band appears in bulk crystals at 1067 cm^{-1}.[28,29]

A new group of three bands at 955, 1080 and 1220 cm^{-1} has developed in sample (b) in well known 4f–4f electronic transitions of Eu^{3+} ($4f^6$) from the ground state $^7F_0$ to the second excited $^7F_2$ multiplet state.[19,30] $^7F_0 \rightarrow {}^7F_2$ transition has a group of a maximum five bands as per the $J = 2$ value of $^7F_2$ state. The ground state $^7F_0$, $J = 0$, is nondegenerate. The first bandgroup occurs in $^7F_0 \rightarrow {}^7F_1$ transition in this series around 300 cm^{-1}. This is not included in the region studied here.

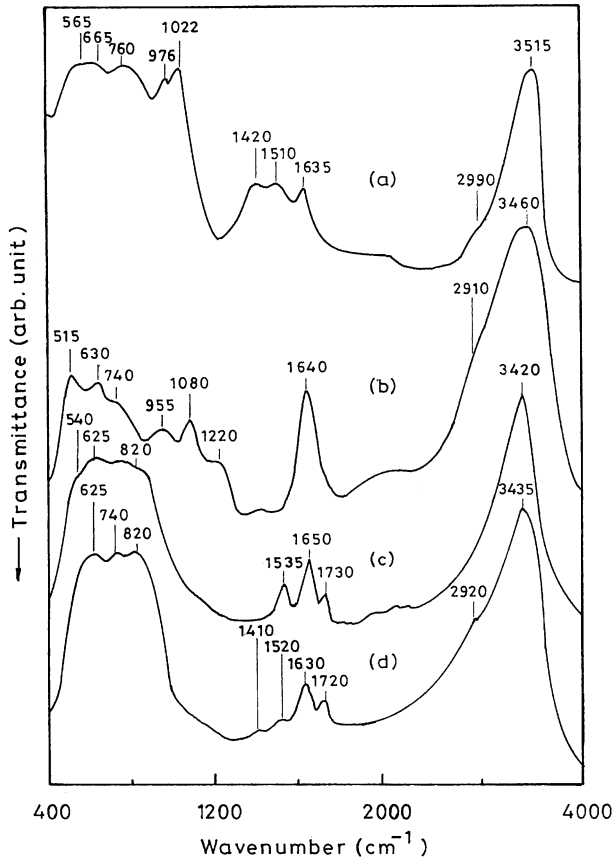

Fig. 11. IR spectra of (a) AlO(OH)·αH_2O and (b) 0.5, (c) 0.5, and (d) 1.5 wt.% Eu^{3+}:Al_2O_3 powders. Spectrum (b) is obtained from as dried powder at 450 K while (c) or (d) is obtained after annealing the sample at 1100 K for 2 h.

Other bandgroups appear at 1640 and 2500 to 4000 cm^{-1} in this sample in prominent band components in the $^7F_0 \rightarrow {}^7F_3$ and $^7F_0 \rightarrow {}^7F_4$ transitions, respectively. These bands are overlapping with O–H bending and stretching vibrations in trace of H_2O in the sample. In water, they appear in a single band at 1640 cm^{-1} and a group of two or three bands at 3100–3600 cm^{-1}.[19] According to it, porous Eu^{3+}:Al_2O_3 powder behaves to be highly susceptible to H_2O adsorption. It has a significant H_2O adsorbed in ambient atmosphere.

The expected resolved band features are obscured in 900–1300 cm^{-1} ($^7F_0 \rightarrow {}^7F_2$ transition) bandgroup by mixing with the nearby Al_2O_3 group vibrations over 400–900 cm^{-1} on dissolving the Eu^{3+} cations in the Al_2O_3 matrix at 1100 K in sample (c) or (d). A strong vibronic coupling occurs between the Al_2O_3 vibration levels and the $^7F_2$ electronic levels and that obscures the features in the pure $^7F_0 \rightarrow {}^7F_2$ electronic transition. As the Eu^{3+} (Eu_2O_3) dissolved in the matrix has no longer a crystalline structure, its discrete $^7F_2$ levels are broadened and merged into a broad unresolved group by mixing with the vibronic levels as per the observed spectrum. A strong band at $\sim$820 cm^{-1} in these samples appears as a result of the vibronic mixing. It belongs to

one of the components in the $^7F_0 \rightarrow {}^7F_2$ electronic transition.

A rather resolved bandgroup of pure electronic bands occurs in the $^7F_0 \rightarrow {}^7F_3$ transition over 1300–1800 cm^{-1} in samples (c) and (d). It consists of three distinct bands at 1535, 1650 and 1730 cm^{-1} in sample (c) while of four bands at 1410, 1520, 1630 and 1720 cm^{-1} in sample (d). A minor variation in number and average positions in the resolved bands is likely in difference in Eu^{3+} contents in the two samples. The content of Eu^{3+} cations determines their macroscopic interactions with the Al_2O_3 matrix on their dissolution in the Eu^{3+}:Al_2O_3 solid solution. Other details of band positions, relative intensities, and assignments of all the observed bands in the various samples are given in Table 2.

3.6. Thermodynamics of Eu^{3+} dissolution in pores

The porous Eu^{3+}:Al_2O_3 powder involves interface between pore wall and particles S_1 and free surface of the particles within pores S_2. That determines a peculiar microstructure of an enhanced Gibb's free energy G_T of the sample before incorporating the Eu^{3+} cations. In a simple case, G_T can be expressed in terms of S_1 and S_2 as follows,

$$G_T = G_V + S_1\sigma_{1+}S_2\sigma_2 \tag{4}$$

where G_V is the equilibrium value of Gibb's free energy of the sample and σ_1 and σ_2 are the energy densities in S_1 and S_2, respectively, at given experimental conditions at ambient temperature and pressure. This excess energy (or volume as can be obtained through first and second laws of thermodynamics) acts as a driving force to dissolve Eu^{3+} particles in pores on heating the sample. It occurs at expense of excess $\Delta G_A = \Delta G_T - \Delta G_A$ (or excess volume ΔV_A) over the equilibrium G_A value in amorphous structure of the sample. Obviously, larger the value of ΔG_A faster is the dissolution of Eu^{3+} particles in pores at reaction temperature. This qualitatively explains why porous Eu^{3+}:Al_2O_3 powder amorphizes at as early temperature as 650 K and recrystallizes into γ-Al_2O_3 at 850 K (1050 K or higher in undoped powder).

The average value of S_1 in sample of volume V can be obtained from average size and volume fraction Φ of pores. Assuming their spherical shape of radius r, it can be expressed as

$$S_{1=}4\pi r^2 N_1 \tag{5}$$

The sample contains $N_1 = \Phi N$ pores and N_2 particles with $N = N_1 + N_2$. In order to compute N_1, let us assume the same size and morphology for the particles and the pores. In this approximation, one can write $N = V \div \frac{4}{3}\pi r^3$. Substituting this value in Eq. (5), we get a simple working relation

$$S_1 = \frac{3\Phi V}{r} \tag{6}$$

Now, let us consider incorporation of particles of size $r' \leqslant r$ in each of the pores. This would add an excess surface area of $3\Phi V r'^2/r^3$ in Eq. (6), i.e. it becomes

$$S_1 \frac{3\Phi V}{r}\left[\frac{r'^2}{r^2}\right] \tag{7}$$

Similar to Eqs. (5) and (6), substituting $N_2 = (1-\Phi)N$ in $S_2 = 4\pi r^2 N_2$, we get

$$S_2 = \frac{3V(1-\Phi)}{r} \tag{8}$$

A combination of Eqs. (7) and (8) yields the total surface energy in a doped porous material

Table 2
Characteristic vibrational or electronic bands observed (in cm^{-1}) in IR spectra of $AlO(OH)\cdot\alpha H_2O$ precursor and Eu^{3+} doped mesoporous Al_2O_3 powders

$AlO(OH)\cdot\alpha H_2O$[a]	Eu^{3+}:Al_2O_3[a]			Assignments
	a	*b*	*c*	
3515 (vs)				O–H stretching
2990 (vw)				AlO(OH)/H_2O
	3460 (vs)	3420 (vs)	3435 (vs)	O–H stretching, H_2O
	2910 (s)		2920 (ms)	$^7F_0 \rightarrow {}^7F_4$ (Eu^{3+})
1635 (w)				Al–O stretching
1510 (w)				AlO(OH) network
1420 (w)				structure
		1730 (vw)	1720 (vw)	
	1640 (s)	1650 (w)	1630 (w)	
		1535 (w)	1520 (vw)	$^7F_0 \rightarrow {}^7F_3$ (Eu^{3+})
			1410 (vw)	
1022 (vs)				Al=O stretching
976 (vs)				AlO(OH)
	1220 (w)			
	1080 (ms)			$^7F_0 \rightarrow {}^7F_2$ (Eu^{3+})
	955 (ms)			
		820 (s)	820 (s)	
760 (vs)				
665 (vs)				AlO(OH) group vibrations
565(vs)				
	740 (s)	740 (s)	740 (s)	
	630 (s)	625 (s)	625 (s)	Al_2O_3 group vibrations
	515 (s)	540 (s)		

[a] The samples, having 0.5, 0.5, and 1.5 wt.% Eu^{3+}, were annealed at (a) 450, (b) 1100 and (c) 1100 K, respectively. Relative band intensities are given in the parentheses; vs: very strong, s: strong, ms: medium strong, w: weak and vw : very weak.

$$\Omega = \frac{3\Phi V}{r}\left[1+\frac{r'^2}{r^2}\right]\sigma_1 + \left[\frac{3V(1-\Phi)}{r}\right]\sigma_2 \quad (9)$$

Assuming $\sigma_1 = \sigma_2 = \sigma$, it simplifies to

$$\Omega = \frac{3V}{r}\left[1+\frac{\Phi r'^2}{r^2}\right]\sigma \quad (10)$$

An observed $\Phi = 0.4$ value, in the Eu^{3+}:Al_2O_3 sample, contributes as much as 37% value of $\Omega = 1.15$ GJ/m^3 at $r = 2.5$ nm and $r' = 2.4$ nm. $\Omega = 1.15$ GJ/m^3 has been estimated using the experimental $\sigma = 0.70$ J/m^2 value.[31] This much excess energy is sufficient enough to maintain a solid in its amorphous state or to induce its phase transformation from an ordered solid to liquid or an amorphous state. As expected, the present value of Ω comes to be larger than a change in G-value by $\Delta G_v = 0.74$ GJ/m^3 in nucleation and growth of a stable Al_2O_3 particle from its liquid state. Note that a nucleus of a solid particle can grow as a stable phase if and only if the total change in G-value dominates over its surface energy. Otherwise, it dissolves in the high energy liquid or amorphous state as in this example of porous Eu^{3+}:Al_2O_3. The result demonstrates the fact that pores with a high surface and/or interface energy in a mesoporous solid play a crucial role to determine its structure at a given temperature.

On heating, Eu^{3+} particles occupying the pores in as received powder react with pore wall and dissolve in Al_2O_3 matrix at expense of interface between pore wall and particles S_1. The release of excess energy ΔG over the equilibrium value G_e in this process can be expressed assuming growth of relative size $\Delta r = r_0 - r$ of particles in pores of initial size r_0 with an empirical relation,

$$\Delta G = \Delta G_m \exp -\left[\alpha\frac{\Delta r}{r_0}\right]^n, \quad \text{with} \quad \Delta r \geqslant 0, \quad (11)$$

where α is a correlation constant which correlates ΔG with pore annihilation and n is an exponent. The value of n depends upon Ω and other parameters. It gives an optimal value of $\Delta G = \Delta G_m$ at $\Delta r = 0$. Actually, it is the temperature which drives Δr according to the sample. It is, therefore, logical to express Eq. (11) in terms of temperature, i.e.

$$\Delta G = \Delta G_m \exp -\left[\alpha'\frac{\Delta T}{T_0}\right]^n, \quad \text{with} \quad \Delta T \geqslant 0, \quad (12)$$

where $\Delta T = T - T_0$, with T_0 the initial temperature of the sample at $r = r_0$.

As portrayed in Fig. 12, Eq. (11) represents a monotonically decreasing value of ΔG as function of $\Delta r/r_0$, with arbitrary values of $\alpha = 1$ and $n = 2$, approaching to a constant G_0 value at $r = r_0$ (2.5 nm). A value of

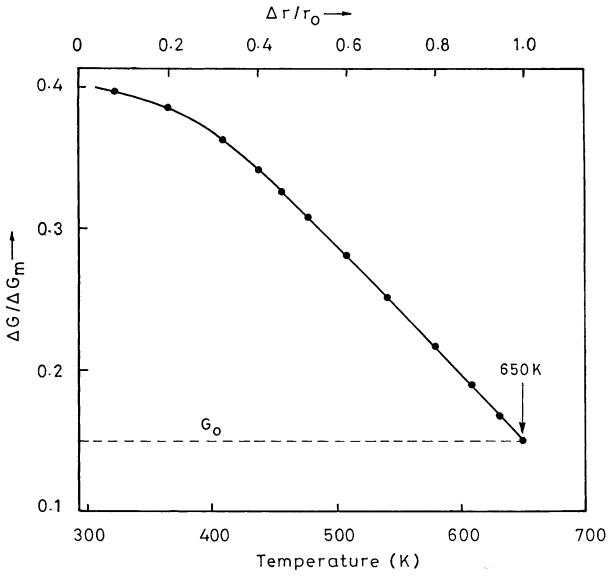

Fig. 12. A model release of excess Gibb's free energy ΔG in porous Eu^{3+}:Al_2O_3 powder as a function of relative particle size $\Delta r/r_0$ in pores. The curve (solid line) is well reproduced (solid points on the curve) assuming annihilation of pores on heating the sample as a function of temperature as per the model.

$G_0 = 0.15\Delta G_m$, assuming 40% excess energy (as per $\Phi \sim 0.4$) in the forms of S_1 and S_2 stored in the sample over the equilibrium bulk value. The obtained curve is well reproduced (solid points) by Eq. (12) with $T_0 = 295$ K and $\alpha' = 0.8\alpha$ (with the same values in the other parameters) so that a stable G_0 value appears at $T_e = 650$ K as per the experimental result of dissolution of Eu^{3+} particles in pores in an amorphous structure. In fact, in a realistic case, the process gets suppressed kinematically by diminished kinetics of involved species as r approaches its equilibrium value r_e. This could reflect in an extended T_s value in a complete transformation as observed at 700 K in the present experiments.

4. Conclusions

Dispersed Eu^{3+} cations in an aqueous $EuCl_3$ solution easily incorporate into the pores on adding in an energized host of hydrogenated mesoporous amorphous $AlO(OH)\cdot\alpha H_2O$ powder (initial porosity Φ is as much as 90% with 10–50 nm average pore diameter[17]) in a closed reactor. The host, which behaves as a reducing agent, converts $EuCl_3$ to Eu_2O_3 as per the reaction, $2\,EuCl_3 + 6\,AlO(OH) \rightarrow Eu_2O_3 + 3\,Al_2O_3 + 6HCl$. The H_2 gas possibly exists in ionized form at pore surface. The sample has a lot of vacancy defects and part of those may be occupied by H^+ cations, or the $[H_3O]^+$ after a reaction with internal H_2O molecules at pores. The $[H_3O]^+$ ions have an activated $2\,EuCl_3 + 3\,[H_3O]^+ \rightarrow Eu_2O_3 + 6HCl + \frac{3}{2}H_2\uparrow$ reaction. This is an efficient spontaneous exothermic reaction which occurs with

evolution of H_2 gas and HCl vapour as per the experimental conditions.

X-ray diffraction of obtained powder, after washing with water and then drying at 450 K, demonstrates formation of an Eu^{3+}:Al_2O_3 solid solution with an amorphous structure of Al_2O_3. The sample has a value of $\Phi \sim 40\%$, determined by difference of its experimental density $\rho = 1.5$ g/cm^3 from the theoretical $\rho = 2.5$ g/cm^3 value and by isothermal sorption of N_2 gas at 77 K. Eu^{3+}(Eu_2O_3) as such exists in C_2/m monoclinic crystal structure (average crystallite size $D \sim 30$ nm) in a thermodynamic equilibrium with amorphous Al_2O_3. Interface between pore wall and particles S_1 and free surface of the particles within pores S_2 determine a high energy thermodynamic state ε of the system far above its equilibrium bulk value ε_0.

If heating the specimen, the excess Gibb's free energy ΔG in the excess $\Delta\varepsilon = \varepsilon - \varepsilon_e$ over the equilibrium value G_e leads to dissolve Eu_2O_3 particles in high S_1 energy pores and results in a complete amorphous Eu^{3+}:Al_2O_3 structure at ~ 700 K. A controlled reconstructive nucleation and growth occurs in γ-Al_2O_3 nanoparticles from the amorphous state in a controlled refined microstructure, with an average $D \sim 5$ nm size of crystallites, at as early temperature as 850 K. The D value hardly improves to 6.5 nm on raising the temperature as high as 1100 K. The Eu^{3+} content is varied up to 1.5 wt.% and the sample is annealed at selected temperatures up to 1100 K in point of view of having a suitable product for applications as lasers, phosphors, and optical and gas sensors. The results are analyzed and modeled in terms of excess ΔG stored in S_1 and S_2 interfaces and surfaces in porous Eu^{3+}:Al_2O_3 powder.

Acknowledgements

The authors gratefully acknowledge the financial support by a research grant from the Aeronautical Research and Development Board, Government of India.

References

1. Reisfeld, R. and Jorgensen, C. K., In *Structure and Bonding*, Vol. 77, ed. R. Reisfeld and C. K. Jorgensen. Springer Verlag, 1992, p. 207.
2. Patra, A., Reisfeld, R. and Minti, H., Influence of aluminium oxide on intensities of Sm^{3+} and Pr^{3+} spectral transitions in sol-gel glasses. *Mater. Lett.*, 1998, **37**, 325–329.
3. Wachtler, M., Speghini, A., Gatterer, K., Fritzer, H. P., Ajo, D. and Bettinelli, M., Optical properties of rare-earth ions in lead germanate glasses. *J. Am. Ceram. Soc.*, 1998, **81**, 2045–2052.
4. Zhang, Y. and Wang, M., The structural information given by R curve of Eu^{3+} probe during the heat treatment process of SiO_2–B_2O_3 gel glasses. *Mater. Lett.*, 1999, **41**, 149–152.
5. Zhang, Y. and Wang, M., A new method to probe the structural evolution during the heat treatment of SiO_2–P_2O_5 gel glasses. *Mater. Sci. Eng. B*, 1999, **67**, 99–101.
6. Nachimuthu, P., Vithal, M. and Jagannathan, R., Absorption and emission spectral properties of Pr^{3+}, Nd^{3+}, and Eu^{3+} ions in heavy-metal oxide glasses. *J. Am. Ceram. Soc.*, 2000, **83**, 597–604.
7. Wang, D. and Wang, M., Research on the phase composition and microstructure of high-efficient phosphor $Sr_2Al_6O_{11}$:Eu^{+2}. *J. Mater. Sci. Lett.*, 1999, **18**, 1433–1435.
8. Ansell, S., Krishnan, S., Weber, J. K. R., Felten, J. H., Nordine, P. C., Beno, M. A., Price, D. L. and Saboungi, M. L., Structure of liquid aluminium oxide. *Phys. Rev. Lett.*, 1997, **78**, 464–466.
9. Tanahashi, J. and Mitsuyu, T., Preparation and optical properties of silica gels in which small gold particles were grown by photoreduction. *J. Non-Cryst. Solids*, 1995, **181**, 77–82.
10. Cai, W., Zhang, T., Jai, J. and Zhang, L., Semiconducting optical properties of silver/silica mesoporous composites. *Appl. Phys. Lett.*, 1998, **73**, 2709–2711.
11. Dickenscheid, W. and Birringer, R., Solid-state reactions in binary mixtures of nanometer-sized particles. *J. Appl. Phys.*, 1995, **77**, 533–539.
12. Johnson, W. L., Thermodynamics and kinetic aspects of the crystal to glass transformation in metallic materials. *Prog. Mater. Sci.*, 1986, **30**, 81–134.
13. Schroder, H., Samwer, K. and Koster, U., Micromechanism for metallic-glass formation by solid-state reactions. *Phys. Rev. Lett.*, 1985, **54**, 197–200.
14. Meng, W. J., Nieh, C. W. and Johnson, W. L., Maximum thickness of amorphous NiZr interlayers formed by a solid-state reaction technique. *Appl. Phys. Lett.*, 1987, **51**, 1693–1695.
15. Zhang, Q., Lai, W. S. and Liu, B. X., Origin of asymmetric growth during solid-state amorphization studied with molecular dynamics simulation. *J. Appl. Phys.*, 2000, **87**, 7696–7701.
16. Schwarz, R. B. and Johnson, W. L., Formation of an amorphous alloy by solid-state reaction of the pure polycrystalline metals. *Phys. Rev. Lett.*, 1983, **51**, 415–418.
17. Ram, S. and Rana, S., Fast surface oxidation induced growth of AlO(OH)·αH_2O molecular fibres at nascent Al-metal surface in ambient atmosphere. *Current Sci.*, 1999, **77**, 1530–1536.
18. Ram, S. and Rana, S., Synthesis of porous Al_2O_3 ceramic clusters by surface hydrolysis of a thin Al-metal plate. *Mater. Sci. and Eng. A*, 2001, **304–306**, 790–795.
19. Ram, S., Electronic Raman and fluorescence spectroscopic studies of Eu^{3+}-doped A_2SO_4·xH_2O sulphates. *J. Raman Spectros.*, 1987, **18**, 537–548.
20. X-ray powder JCPDS diffraction file: 12.387.
21. X-ray powder JCPDS diffraction file: 12.384.
22. X-ray powder JCPDS diffraction file: 29.63.
23. Azaroff, L., *Elements of X-ray-crystallography*. McGraw-Hill, New York, 1968 p. 557.
24. Coffer, J. L., Beauchamp, G. and Zerda, T. W., Porous silica glasses doped with quantum-confined cadmium selenide. *J. Non-Cryst. Solids*, 1992, **142**, 208–214.
25. Kanemitsu, Y., Luminescence properties of nanometer-sized Si crystallites: core and surface states. *Phys. Rev. B*, 1994, **49**, 16845–16848.
26. Banerjee, S. and Chakravorty, D., Optical absorption of composites of nanocrystalline silver prepared by electrodeposition. *Appl. Phys. Lett.*, 1998, **72**, 1027–1029.
27. Shannon, R. D., Revised effective ionic radii and systematic studies of interatomic distances in halides and chalcogenides. *Acta Cryst.*, 1976, **A32**, 751–767.
28. Ram, S., Infrared spectral study of molecular vibrations in amorphous, nanocrystalline and AlO(OH)·αH_2O bulk crystals. *Infrared Phys. and Technol.*, in press.
29. Fripiat, J. J., Bosmans, H. and Rouxhet, P. G., Proton mobility

in solids. I. Hydrogen vibration modes and proton delocalization in boehmite. *J. Phys. Chem.*, 1967, **71**, 1097–1111.
30. Ram, S. and Sinha, S. K., Luminescence characteristics and electronic levels of Eu(III) in N,N-Dimethyl-diphenyl-phosphinamide (DDPA) adduct of europium perrhenate. *J. Solid State Chem.*, 1987, **66**, 225–234.
31. DeHoff, R. T., *Thermodynamics in Materials Science*. McGraw-Hill International Edition, Singapore, 1993 pp. 19–35.